Appl. Phys. B 87, 649–653 (2007)
DOI: 10.1007/s00340-007-2645-3

Applied Physics B
Lasers and Optics

X. LIANG[1]
J. BARTSCHKE[2]
M. PELTZ[1]
J.A. L'HUILLIER[1,✉]

Non-collinear nanosecond optical parametric oscillator based on periodically poled LN with tilted domain walls

[1] University of Kaiserslautern, Physics Department, Erwin-Schroedinger-Strasse 46, 67663 Kaiserslautern, Germany
[2] Xiton Photonics GmbH, Opelstrasse 10, 67661 Kaiserslautern, Germany

Received: 21 November 2006/Revised version: 13 March 2007
Published online: 16 May 2007 •

ABSTRACT We report on a non-collinear, 1064 nm pumped, 10 kHz repetition rate ns-OPO which consists of a 13 mm long periodically poled lithium niobate (PPLN) crystal in a hemispherical optical cavity. The non-collinear phase-matching is achieved by tilting the domains by 60° with respect to the pump beam. This phase-matching avoids back conversion of signal and idler radiation into pump radiation and thus improves the spatial quality of the generated OPO radiation considerably. At a pump power of 5.5 W the OPO provided a conversion efficiency of up to 34%. The generated OPO pulses with a total power of up to 1.85 W were emitted in an almost diffraction limited beam with a M^2-value of 1.1. The beam quality did not change when the pump power was varied in the range of 2–5 W.

PACS 42.65.-k; 42.65.Yj

1 Introduction

Optical parametric oscillators (OPOs) are widely used as tunable sources of coherent radiation for many applications like spectroscopy or remote sensing [1, 2].

A basic problem of highly efficient OPOs is the spatial quality of the generated beams of signal and idler radiation. The beam quality usually decreases with an increasing pump power. This is mainly due to back conversion of signal and idler radiation into pump radiation [3, 4]. Although the beam quality was improved substantially to an M^2-value of 2.5 by using a confocal unstable resonator it is still severely limited by the back conversion process [5]. Especially OPOs with high gain, like pulsed OPOs or OPOs based on quasi-phase-matched (QPM) crystals, suffer from this problem [4, 6]. Further techniques to improve the beam quality of nanosecond OPOs like image rotation [7, 8] have been proposed and demonstrated. But these techniques work only for birefringence phase-matched OPOs and can hardly be applied to quasi-phase-matched OPOs.

Since the first demonstration of an OPO in PPLN by Myers et al. [9] in 1995, several OPOs based on QPM crystals have been demonstrated. The main advantages of those crystals are the designable phase-matching characteristics and the large effective non-linearity.

A well-known method for improving the spatial beam quality is the use of a non-collinear phase-matching geometry. In this case the laser beam and the generated waves do not propagate in the same direction and therefore back conversion is strongly reduced. In the past non-collinear geometries have been reported for several non-linear systems. A non-collinear setup was demonstrated, e.g., for an OPO based on periodically poled $KTiOPO_4$ (PPKTP) [10, 11]. For PPLN non-collinear optical parametric oscillation has been obtained by rotating the crystal [12] or the pump beam [13, 14] with respect to the cavity axis. The main objective for the non-collinear operation of these devices was to improve the tunability or to broaden the spectral bandwidth. Non-collinear difference frequency generation (DFG) was used also for the generation of terahertz radiation in order to reduce the high intrinsic absorption [15]. In these investigations the non-collinear phase-matching widened the tuning range, minimized the absorption and improved the OPOs conversion efficiency.

In this paper we report on a non-collinear phase-matched OPO which provides an optimized spatial quality for both the signal and the idler beam. In this OPO the non-collinear phase-matching is realized by using a PPLN crystal with domains which are tilted (TPPLN) by an angle of 60° with respect to the pump beam. The experimental results are compared with those obtained for a collinear beam propagation. The OPO operated with a TPPLN crystal shows a substantial improvement in both the beam quality and the conversion efficiency.

2 Design and preparation of the PPLN and TPPLN crystals

In Fig. 1a the wavevector diagrams for the standard collinear phase-matching scheme (upper) and the non-collinear geometry (lower) are shown. For the collinear scheme the wavevectors fulfill the following equation:

$$\boldsymbol{k}_\mathrm{g} + \boldsymbol{k}_\mathrm{s} + \boldsymbol{k}_\mathrm{i} = \boldsymbol{k}_\mathrm{p}\,, \tag{1}$$

where $\boldsymbol{k}_\mathrm{p}$, $\boldsymbol{k}_\mathrm{s}$ and $\boldsymbol{k}_\mathrm{i}$ are the wavevectors of the pump, signal and idler wave, respectively. The term $\boldsymbol{k}_\mathrm{g}$ denotes the wavevector ($|\boldsymbol{k}_\mathrm{g}| = 2\pi/\Lambda$) provided by the QPM structure

✉ Fax: +49-631-2053906, E-mail: huillier@physik.uni-kl.de

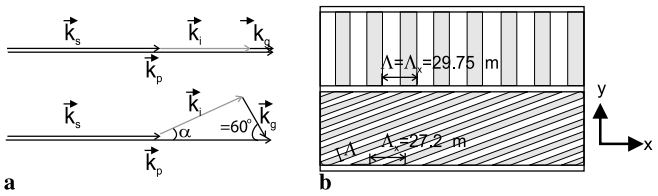

FIGURE 1 (**a**) Wavevector diagrams for collinear and non-collinear phase-matching. (**b**) Periodic structure of the PPLN for collinear and non-collinear OPO systems

with the period Λ. For a non-collinear propagation of the idler wave the conservation of momentum requires an additional wavevector component perpendicular to the direction of propagation. In a TPPLN this component is obtained by the tilt of the periodic structure as shown in the lower part of Fig. 1a. The direction of the pump and the signal wave are determined by the direction of the pump beam and the signal resonant OPO cavity, respectively. The laser and signal waves are collinear and therefore $\boldsymbol{k}_\mathrm{g}$ causes a non-collinear propagation of the idler wave. For this geometry (1) has to be modified in the following way:

$$|\boldsymbol{k}_\mathrm{g}|\cos\theta + |\boldsymbol{k}_\mathrm{s}| + |\boldsymbol{k}_\mathrm{i}|\cos\alpha = |\boldsymbol{k}_\mathrm{p}|\,, \tag{2}$$

where α is the angle between the signal wave and the idler wave. The angle α is related to the angle θ between the propagation direction of the pump and signal wave and the direction of the wavevector $\boldsymbol{k}_\mathrm{g}$ in the following way:

$$|\boldsymbol{k}_\mathrm{g}|\sin\theta = |\boldsymbol{k}_\mathrm{i}|\sin\alpha\,. \tag{3}$$

In order to compare the properties of a collinear and non-collinear OPO it is useful to perform the experiments with the same crystal to ensure that the results are not influenced by differences in crystal properties. This can be achieved by using a crystal which contains tilted and untilted domain structures.

$LiNbO_3$ itself exhibits a threefold rotation symmetry about its c-axis [16] and shows a tendency for generating 180° domains with a hexagonal shape and walls parallel to the y-axis or with an angle of ±60° with respect to the y-axis [17]. Because of this fact we used the domains produced under an angle of 60° for the non-collinear TPPLN-OPO.

Figure 1b shows the periodic structure of the crystal used for collinear and non-collinear OPO operation. The letters x, y and z denote the principal axes of the crystal with the z-axis chosen parallel to the polar axis (c-axis) of LN [16]. In the experiments a 13-mm-long and 0.5-mm-thick PPLN crystal has been used which contains 1.7-mm-wide parallel gratings with an angle of 0° and 60° with respect to the crystal y-axis. To obtain the same wavelength with the tilted and untilted gratings the corresponding poling periods were determined from (1) and (2). The poling period along the x-axis was $\Lambda_x = 27.2\,\mu\mathrm{m}$ for the tilted periods and $\Lambda_x = 29.75\,\mu\mathrm{m}$ for the grating for normal incidence of the pump and signal radiation. For the grating for normal incidence the grating period is equal to Λ_x, while the poling period along the x-axis Λ_x results from the grating period Λ according to $\Lambda = \Lambda_x\cos(\theta)$ (see Fig. 1).

The poling of the crystal was performed using the standard electric-field domain-reversal technique [18]. The etched surface confirms that both structures have uniform domain walls and a duty cycle which is close to 50%. Both crystal facets were polished.

3 Experimental setup

A scheme of the experimental setup is shown in Fig. 2. The pump source is a 1064 nm TEM_{00} diode-pumped Q-switched Nd:YVO_4 oscillator–amplifier system, which provides 6-ns-long pulses with a repetition rate of 10 kHz and an average output power of 7 W. The spatial beam profile was almost diffraction-limited with a M^2-value of 1.2. The pump power was varied by an attenuator, consisting of a half-wave plate and a thin-film polarizer.

The OPO resonator was a hemispherical optical cavity with a mirror separation of 34 mm. The input coupler (IC) of the OPO cavity is a flat mirror AR coated for the pump and HR coated for the signal wavelength in the range of 1500 and 1700 nm. A concave CaF_2 mirror with a radius of curvature of 75 mm and a reflectivity of $R = 70\%$ for the signal wave was used as the output coupler (OC). The focusing of the pump beam was matched to the mode size in the OPO cavity using a single lens with a focal length of $f = 200$ mm. The OPO cavity contained the PPLN crystal described in the previous section. To avoid photorefractive effects the crystal was heated to 150 °C. The optical parameters of the OPO like the output power, beam quality and the wavelength were measured using a power meter (Melles Griot, 30 W Broadband Power/Energy Meter), a CCD camera (Spiricon Inc., LBA-PC), a beam scope (Merchantek, Beamscope) and a spectrometer (ANDO, Optical Spectrum Analyzer AQ6315A).

4 Experimental results

4.1 *Output power and efficiency*

Figure 3 shows the output power (Fig. 3a) and the conversion efficiency (Fig. 3b) in dependence of the pump power measured for both the collinear and non-collinear OPO. The collinear OPO shows a threshold of 0.4 W and a maximum conversion efficiency of $\eta = 32.5\%$. For pump powers exceeding 2 W, the efficiency saturates because of back conversion of signal and idler radiation into pump radiation. The slope efficiency is 34% for the collinear and 54% for the non-collinear OPO. Compared to the collinear OPO the threshold of the non-collinear OPO is considerably higher. On the other hand the conversion efficiency increases with the pump power to more than 35% for pump powers exceeding 5.5 W. The effective non-linearity d_eff is the same for the collinear and the non-collinear geometry, since all waves are polarized parallel to the c-axis and the non-collinear propa-

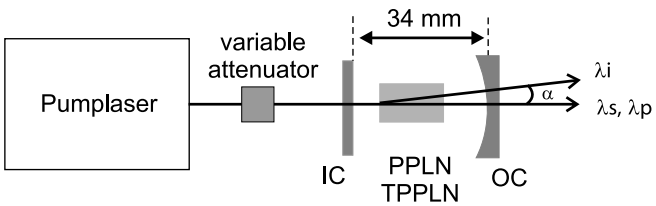

FIGURE 2 Sketch of the experimental setup (for details see text)

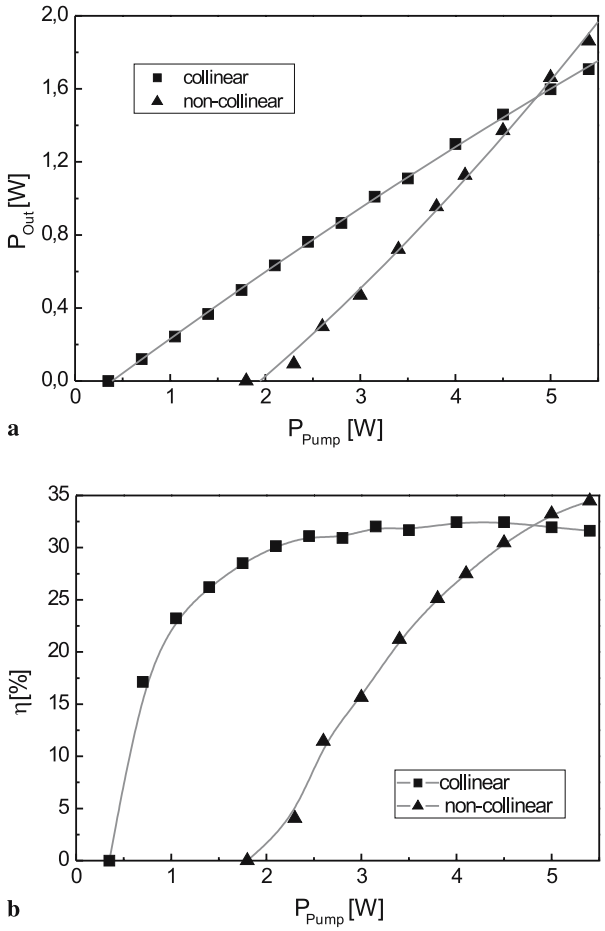

FIGURE 3 (**a**) Average power of the signal and idler waves measured in dependence of the pump power. (**b**) Conversion efficiency calculated from the results shown in (**a**)

gation occurs in a plane perpendicular to the *c*-axis. Thus the observed changes in the threshold can be attributed to the spatial walk off due to the non-collinear propagation and possible residual back reflection of the idler wave. The improved efficiency of the non-collinear OPO compared to the collinear OPO can be attributed to the reduced back conversion. These results indicate that the non-collinear OPO provides a higher output power and efficiency in comparison to the standard collinear OPO.

A critical phenomena for powerscaling of PPLN-OPOs is the green induced infrared absorption (GRIIRA) [19] and the absorption of the idler radiation at wavelengths beyond $\approx 4.5\,\mu$m. Because of this absorption the output facet of the crystal was damaged for the collinear PPLN-OPO for pump powers exceeding 5.5 W. This was not the case for the non-collinear TPPLN-OPO, a fact which may indicate an additional advantage of the non-collinear OPO. The higher damage threshold may result from the fact that the second harmonic of pump, idler or parasitic radiation generated at other wavelengths are not emitted in the same direction as the pump and signal wave. Therefore the total power density on the output facet of the crystal is lower.

Since we were mainly interested in a direct comparison of the PPLN and TPPLN geometry with respect to the beam profile and back conversion we limited the maximum pump power for the further experiments to 5.3 W, in order to avoid further damaging the crystal.

4.2 *Beam quality*

A major goal of this study was to improve the quality of the OPO beams at high pump powers. Thus the beam quality and its dependence on the pump power was measured for both the collinear and non-collinear scheme.

In order to obtain reliable values for M^2 the beam profile of the signal radiation was measured in the x- and y-directions at several positions close to the beam waist and in the far field. The beam radii were calculated from these positions where the intensity distribution decreased with respect to its maximum by a factor of $1/e^2$. From the values of the beam radii

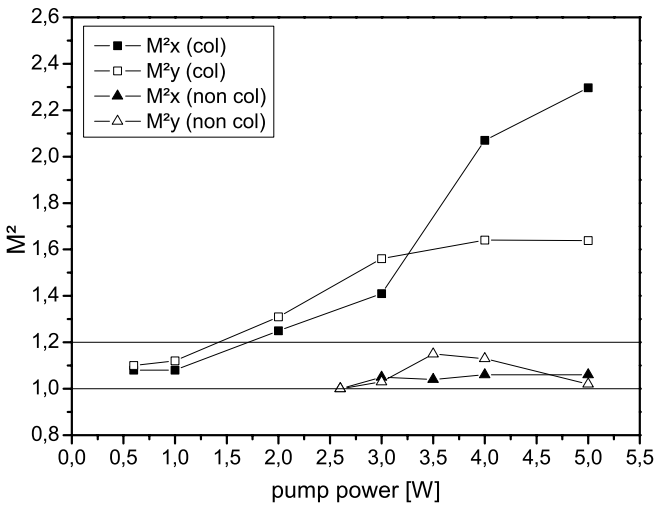

FIGURE 4 Experimentally obtained M^2-values for the signal wave in dependence of the pump power for the collinear (*filled squares*) and the non-collinear OPO (*filled triangles*)

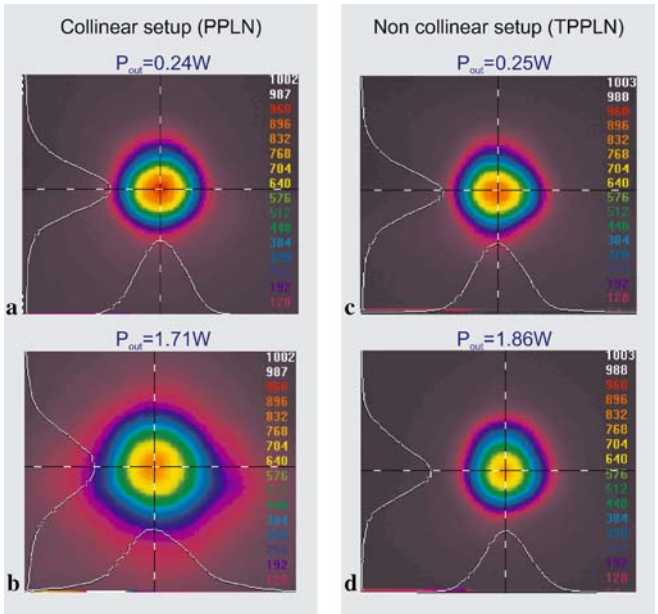

FIGURE 5 Measured far-field 2D beam profiles of the signal wave of the collinear OPO (**a**,**b**) and the non-collinear OPO (**c**,**d**) for different output powers

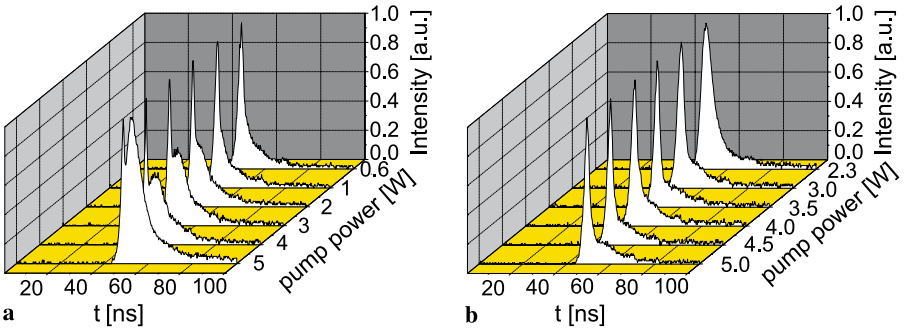

FIGURE 6 Temporal profiles of the transmitted pump pulses measured at different pump power levels for (**a**) the collinear OPO and (**b**) the non-collinear OPO

the M^2-values were obtained by fitting the beam size $w(z)$ of a multimode Gaussian beam to the data where

$$w(z) = w_0\left[1 + M^2\left(\frac{\lambda}{\pi w_0^2}\right)^2 (z - z_0)^2\right]^{\frac{1}{2}} \quad (4)$$

and M^2 is the fit parameter. Figure 4 shows the obtained M^2-value for the x- and y-direction of the signal beam in dependence of the pump power for both the collinear (filled squares for the x-direction, open squares for the y-direction) and the non-collinear OPO (filled triangles for the x-direction, open triangles for the y-direction). It is seen that for the collinear PPLN-OPO the M^2-value of the signal beam increases from 1.1 to 2.28 (x-direction) and 1.65 (y-direction) when the pump power is increased from 0.6 to 5 W. In contrast to this behavior, the M^2-value for both directions of the non-collinear TPPLN-OPO remains almost constant with a value of less then 1.2 for pump powers up to 5 W. This observation is confirmed by the two-dimensional far-field distribution recorded by a CCD camera as shown in Fig. 5.

In order to investigate and compare the back conversion for the collinear and the non-collinear OPO, the temporal shape of the pump pulse was examined. Figure 6 shows the measured pulse shapes for different pump powers ranging from 0.6 to 5 W for the collinear and non-collinear geometry, respectively. To allow a comparison of the pulse shapes at different pump powers, the measured pulse powers were normalized to the same maximum level.

From Fig. 6a it is obvious that for pump powers exceeding 2 W back conversion occurs in the collinear OPO, because shortly after reaching the threshold and depleting the pump, the pump intensity increases again with time. This causes a degradation of the beam quality and saturates the efficiency. This effect becomes stronger with an increasing pump power. In contrast to the collinear OPO the envelope of the transmitted pump pulses shows no minimum for the non-collinear OPO. This indicates that back conversion is not observed for all applied pump powers. This is in agreement with the observation that the M^2-value of the signal beam did not change with pump power and the conversion efficiency did not saturate.

4.3 *Wavelength tuning*

The periodic structure used for collinear and non-collinear operation were designed using the Sellmeier equation given in [20] in order to provide the same signal wavelength λ_s. In full agreement with the design goal the measured λ_s was 1571 nm and 1566 nm for the collinear and the non-collinear OPO, respectively. For the non-collinear OPO the angle between the pump and idler wave has been measured as 0.22 rad. This corresponds to an angle of 0.101 rad inside the crystal which is in good agreement to the value of 0.1 rad obtained by (3).

Conventionally the wavelength tuning is done by adjusting the temperature or the poling period. But tuning can also be achieved by rotating the QPM crystal or the cavity. Both result in a non-collinear propagation of the interacting waves. Non-collinear optical parametric processes have been investigated in the past in order to enhance the tunability and broaden the bandwidth [12, 13]. In these investigations a wavelength tuning range of 1563 to 1810 nm has been demonstrated [14] for a rotation of 4°. Beside the wavelength, the spectral bandwidth also changed considerably from 8.5 to 300 nm. In these investigations an OPG/OPO process with a rotated pump beam or a crystal with the OPO mirrors on its surfaces has been used and therefore all three waves propagated in a different direction. Opposite to this behavior, in our setup the signal and pump wave remain always collinear, even when the crystal is rotated.

In order to compare the frequency tuning by rotating the crystal for the collinear and the non-collinear geometry the rotation angle has been systematically varied in the range of

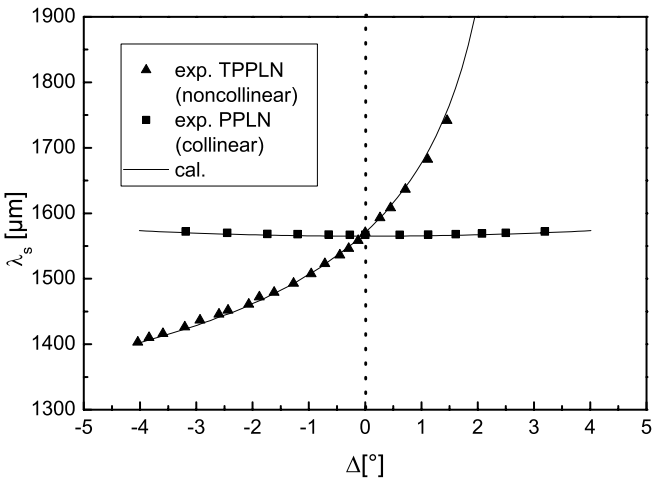

FIGURE 7 The signal wavelength of the TPPLN and PPLN-OPO measured for different rotating angles Δ of the crystal with respect to the propagation direction of the pump radiation. In addition to the experimental data for the collinear (*filled squares*) and the non-collinear OPO (*filled triangles*) the theoretically calculated tuning curves (*solid lines*) are plotted

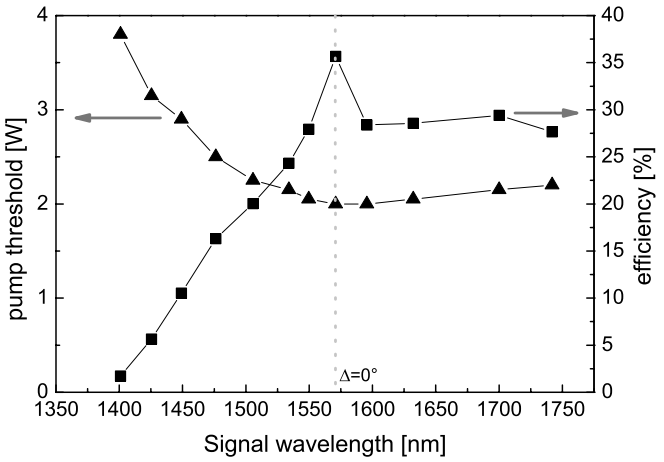

FIGURE 8 The pump threshold and efficiency depending on the signal wavelength measured for different rotating angles Δ of the crystal with respect to the propagation direction of the pump radiation

$\Delta = -4°$ to $\Delta = +4°$. The measured wavelength tuning is shown in Fig. 7 for both geometries. For a comparison with the theory the calculated tuning curve is also plotted for the collinear and non-collinear geometry (solid line). The curves have been calculated from (2) and (3) under the assumption that the signal and pump wave are still collinear. The additional angle Δ has been considered in the calculation within the angle $\theta_{\text{eff}} = \theta + \Delta$ between the pump wave and the grating vector. Both schemes show a good agreement between the calculation and the measurement. As seen from this figure the tuning range of the signal wavelength of the non-collinear OPO extends from 1402 to 1742 nm for a crystal rotation of 5.45°. In contrast to this behavior the signal wavelength of the collinear OPO is almost constant and independent of the crystal's orientation.

Figure 8 shows the dependency of the measured pump threshold (left axis) and efficiency (right axis) on the signal wavelength obtained by rotating the crystal. The pump threshold decreases and the efficiency increases with an increasing wavelength up to a wavelength of approximately 1550 nm and remains almost constant beyond this wavelength. This indicates that the wavelength tuning may not affect the pump threshold, the efficiency and the output power of the OPO at least for wavelengths beyond 1550 nm. The behavior at shorter wavelength is mainly attributed to an increase of the angle between the signal and the idler wave, which reduces the gain.

5 Conclusion

In conclusion, we have demonstrated, to our knowledge for the first time, that a non-collinear OPO of a periodically poled crystal with domains tilted by an angle of 60° provides higher beam quality, a higher conversion efficiency and a wider tuning range compared to an OPO with a standard PPLN crystal with domains perpendicular to the propagation of the pump wave. The measured optical properties are summarized and compared in Table 1. This comparison clearly indicates that a TPPLN-OPO is superior to a standard PPLN-OPO with respect to important optical parameters.

	PPLN (collinear)	TPPLN (non-collinear)
Tilt angle	0°	60°
Conversion efficiency	32.5%	34.5%
Slope efficiency	33.9%	53.1%
Pump threshold	0.4 W	2 W
Back conversion	Dominant	Strongly reduced
M^2	1.08 (@0.6 W)–2.28 (@5.5 W)	< 1.2
Tuning range	1566–1579 nm	1402–1742 nm

TABLE 1 Comparison of the optical parameters measured for the PPLN and TPPLN-OPO

ACKNOWLEDGEMENTS The authors would thank J.P. Meyn for preparing the PPLN crystal, U. Bäder for helpful discussions and R. Wallenstein for his continuous support and various instructive discussions.

REFERENCES

1 G.M. Gibson, M. Ebrahimzadeh, M.J. Padgett, M.H. Dunn, Opt. Lett. **24**, 397 (1999)
2 T.H. Allik, S. Chandra, W.W. Hovis, C.G. Simi, J.A. Hutchinson, Proc. SPIE **3383**, 58 (1998)
3 S.C. Lyons, G.-L. Oppo, W.J. Firth, J.R.M. Barr, IEEE J. Quantum Electron. **QE-36**, 541 (2000)
4 G. Anstett, M. Nittmann, R. Wallenstein, Appl. Phys. B **79**, 305 (2004)
5 G. Hansson, H. Karlsson, F. Laurell, Appl. Opt. **40**, 5446 (2001)
6 G. Anstett, A. Borsutzky, R. Wallenstein, Appl. Phys. B **76**, 541 (2003)
7 A.V. Smith, M.S. Bowers, J. Opt. Soc. Am. B **18**, 706 (2001)
8 A.V. Smith, D.J. Armstrong, J. Opt. Soc. Am. B **19**, 1801 (2002)
9 L.E. Myers, G.D. Miller, R.C. Eckardt, M.M. Fejer, R.L. Byer, W.R. Bosenberg, Opt. Lett. **20**, 52 (1995)
10 J.-P. Fève, O. Pacaud, B. Boulanger, B. Ménaert, J. Hellström, V. Pasiskevicius, F. Laurell, Opt. Lett. **26**, 1882 (2001)
11 M. Tiihonen, V. Pasiskevicius, F. Laurell, Opt. Express **12**, 5526 (2004)
12 M.J. Missey, V. Dominic, P.E. Powers, K.L. Schepler, Opt. Lett. **24**, 1227 (1999)
13 S.T. Yang, S.P. Velsko, Opt. Lett. **24**, 133 (1999)
14 C.-W. Hsu, C.C. Yang, Opt. Lett. **26**, 1412 (2001)
15 Y. Sasaki, A. Yuri, K. Kawase, H. Ito, Appl. Phys. Lett. **81**, 3323 (2002)
16 R.S. Weis, T.K. Gaylord, Appl. Phys. A **37**, 191 (1985)
17 G.D. Miller, Dissertation, Stanford University (1998)
18 M. Yamada, N. Nada, M. Saitoh, K. Watanabe, Appl. Phys. Lett. **62**, 435 (1993)
19 Y. Furukawa, K. Kitamura, A. Alexandrovski, R.K. Route, M.M. Fejer, G. Foulon, Appl. Phys. Lett. **78**, 1970 (2001)
20 D.H. Jundt, Opt. Lett. **22**, 1553 (1997)